Simulation of Ultrasonic Array Imaging of Composite Materials With Defects

Yousif Humeida, Valerie J. Pinfield, Richard E. Challis, Paul D. Wilcox, and Chuan Li

***Abstract*—Ultrasonic transducer arrays are extensively used for the nondestructive evaluation of materials for aerospace and other applications. However, their use with composites requires some technique development because of reflections at the layer boundaries and the effects of attenuation. When used in full matrix capture mode, algorithms such as the total focusing method (TFM) must be applied to obtain the image. In composite materials, improvement to the algorithm is required to include the effects of material anisotropy (affecting wave speed) and optimum aperture limits to optimize the signal-to-noise ratio and location detection for a defect in the material. This paper presents simulations of the ultrasonic array signals in multilayer anisotropic materials with and without a simulated defect. A kernel model for plane wave propagation in the material is combined with an angular spectrum decomposition (for finite transducer elements) and transducer frequency response, to model the full array signals. Inclusion of the defect is through its far-field scattering response. The model facilitates the study of imaging algorithm development by identification of the effects of anisotropy, signal-to-noise ratio, and aperture limit. An analytical method for the calculation of the effective group velocity in the composite at low frequency is demonstrated, permitting rapid calculation of time delay laws in practice.**

I. Introduction

The increasing use of ultrasonic phased arrays in the inspection and testing of composite materials brings with it the importance of developing ultrasonic signal processing techniques that will achieve better imaging and inspection performances by maximizing efficiencies and/or minimizing computational requirements while improving resolution and image quality. Holmes *et al.* [1] and Drinkwater and Wilcox [2] have developed several signal processing techniques for ultrasonic array imaging in metals, including the use of full matrix capture (FMC) and the total focusing method (TFM), an algorithm for obtaining images at optimum resolution. However, the application of such techniques in composite materials is more challenging, because of their multi-layered structure and their anisotropic and inhomogeneous properties. To apply the TFM technique for planar multilayer composites, it is necessary to make some modifications, such as the use of a directionally-dependent velocity to account for anisotropy, and an aperture angle limit to eliminate some contributions from reflections at ply boundaries. These modifications have been explored experimentally and are reported in a previous paper [3]. The need arises to simulate the propagation of ultrasonic signals in composites, not only to validate and confirm the results shown in [3], but also to study and analyze, using computational models, the behavior of ultrasonic array signals in such anisotropic multilayer composite materials, and to inform future algorithm development.

A variety of approaches are reported in the literature for the simulation of ultrasonic signals in composites, or other anisotropic multi-layered materials. A ray-tracing technique has been implemented using homogenization to account for the layered character of the material by Deydier *et al.* [4]. This has the advantage of being applicable to nonplanar geometries, but does not show the structural reflections from plies. An alternative technique proposed by Huang *et al.* [5] uses multi-Gaussian beams to propagate through the structure, accounting for changes to the beams at ply interfaces, and simulating the signal from finite transducer array elements by several such multi-Gaussian beams. The method can be used for planar or nonplanar composites, but is computationally intensive. An alternative is to constrain the problem to planar materials, to exploit the highly efficient plane-wave models established in the seismology literature [6]–[15]. These are able to account for reflection and refraction at layer interfaces, mode conversion, and anisotropic material properties, and have been optimized for speed and accuracy. As such, they offer an ideal basis for the simulation of transducer array signals. These methods have been adopted by Mienczakowski *et al.* [16] with some success, but with a restriction to normal incidence signals. Pialucha and Cawley [17] also implemented a plane wave model, combining it with the angular spectrum method to simulate transducer signals. However, their model considers only isotropic materials. In the current work, we have adopted a plane wave model for anisotropic materials as the kernel of the simulation, together with the angular spectrum method to simulate the finite beams from array elements.

Acoustic plane waves in multilayer media are usually studied using matrix methods. Thomson [6] and Haskell [7] have developed the transfer matrix method, which is considered the classical way of solving such problems. An alternative is the global matrix method developed by Knopoff [8], which solves the instability problems of the transfer matrix especially for large frequency/thickness (fd) products. The transfer matrix for general anisotropic

Manuscript received February 22, 2013; accepted June 17, 2013. This work was supported by the UK Research Centre in NDE Targeted Programme, by the Engineering and Physical Sciences Research Council (grant number EP/H01196X/1), Airbus, and Rolls Royce.

Y. Humeida, V. J. Pinfield, and R. E. Challis are with the Electrical Systems and Optics Division, University of Nottingham, Nottingham, UK (e-mail: Richard.Challis@nottingham.ac.uk).

P. D. Wilcox and C. Li are with the Department of Mechanical Engineering, University of Bristol, Bristol, UK.

DOI http://dx.doi.org/10.1109/TUFFC.2013.2778

media was developed by Nayfeh [9], [10]. Lowe [11] has published a review of the different matrix techniques in multilayer media. More recently, Wang and Rokhlin [12]–[15] introduced the recursive stiffness matrix method, in which a recursive algorithm uses individual layer stiffness matrices to form a global stiffness matrix for the whole material. This method achieved stable results with the same efficiency as the transfer matrix method. Hosten and Castaings [18] used a similar technique to develop a recursive surface impedance matrix. For the purposes of this study, a model for the plane waves in generally anisotropic multilayer media was developed using the recursive stiffness matrix technique. The stiffness matrix method will be used throughout this paper to carry out plane wave calculations.

The plane wave solution for multilayer media does not accurately reflect real situations in which the transducers used for transmitting/receiving the ultrasonic waves are of finite dimensions, and hence bounded beam acoustic signals, rather than plane waves which extend infinitely along the interfaces, must be considered. Different methods can be used to model diffraction of bounded beams; the angular spectrum method is one of them. This method states that the fields (stresses or displacements) anywhere in the considered space can be defined uniquely and completely by the sum of an infinite number of plane waves in different directions [19], [20]. As an example, Rehman *et al.* [21] used the angular decomposition of plane waves to calculate the reflection profile of bounded beams from anisotropic multilayer media.

Modeling localized defects in such multilayer composite materials has also been considered. To study the response of a specific defect or scatterer to acoustic waves, it is necessary to calculate the diffraction of waves from the transmitting transducer through the material to the defect and from the defect back to the receiving transducer, and, furthermore, to combine that with a defect scattering model, which describes how the defect interacts with the incident acoustic waves [22]. Side-drilled holes (SDHs) have been considered in this study because they are the standard type of scatterers used to evaluate ultrasonic nondestructive testing techniques.

Many authors have developed techniques to study the scattering of acoustic waves from different kinds of defects in different types of materials. Lopez-Sanchez *et al.* [23] have considered a pulse–echo measurement system model for an SDH embedded in a single isotropic layer. In this work, two methods have been used for the scattering model: the separation of variables solution and the Kirchhoff approximation. The Kirchhoff approximation is only valid at high frequencies or for large SDHs (i.e., when $ka > 1$, where k is the wavenumber and a is the SDH radius). Niklasson and Datta [24] have developed solutions using the separation of variables to the scattering from an infinite transversely isotropic cylinder in a transversely isotropic medium. The special cases in which the cylinder is an isotropic material or a cavity were also considered. Analytical solutions for the scattering behavior of SDHs at different angles in general anisotropic material have not yet been developed, to the our knowledge, and they have only been studied using numerical methods such as the finite element (FE) method [25]–[27]. For scatterers in multilayer systems, Zhang *et al.* [27] have provided a hybrid model that uses ray-based calculations for the system model and FE measurements for the scattering model. In this work, the layers in which the SDH lies have been modeled as a single effective homogeneous medium—an assumption that holds for low-frequency acoustic waves (i.e., high wavelength-to-thickness ratios, λ/d) [28], [29]. For many applications, such as the calculation of group velocities or modeling of SDHs in composite, such an assumption is very useful. Backus [30] has developed formulas for the calculation of the equivalent homogeneous properties for isotropic or transversely isotropic layers, and these can be easily adapted to generally anisotropic layers, as has been done by Milton [31].

This work reports simulations of full transducer array data for planar composite materials with anisotropic properties, including embedded defects in the form of an SDH. The simulations combine several modeling techniques to achieve this end, adopting highly efficient plane-wave models originally developed for seismological purposes, together with angular spectrum decomposition to model the finite beams produced by transducer array elements, and combining these with the scattering characteristics of a defect. A method for estimating the effective properties of a layered structure has also been used for the calculation of group velocities through the composite at low frequency. The results of the simulations have been used to evaluate proposed image processing algorithms for FMC data sets obtained from composites. Two such examples of imaging improvements are explored in this paper; they are the use of an angle-dependent group velocity to estimate time delays between transducer array elements and imaging points, and the application of an aperture angle limit to improve the signal–to–coherent-noise ratio for defect detection.

II. Modeling Waves in Multilayer Anisotropic Media

A. Plane Wave Model in Multilayer Media

This section summarizes the kernel plane wave model, based on the work of Wang and Rokhlin [12]–[15], implemented as Matlab code (The MathWorks Inc., Natick, MA) by M. Castaings and B. LeCrom of the University of Bordeaux 1. Let us assume that a plane wave is incident on a planar multilayer structure which consists of n homogeneous, anisotropic layers and is of infinite extent in the directions normal to the through-thickness direction (Fig. 1). The structure is bounded by two semi-infinite regions, which are labeled layer 0 and layer $n + 1$ and considered to be homogeneous anisotropic materials, with the specific example of a nonviscous fluid (i.e., water) being

considered as a special case. A plane wave is assumed to be traveling in the upper half-space and enters the system at the origin of the global coordinate axes system [$\mathbf{x} \equiv (x_1, x_2, x_3)$] having an incident angle of θ with the x_1-axis; its wavevector projection on the x_2-x_3 plane is assumed to have an arbitrary angle of ϕ with the x_2 axis. A harmonic solution for plane wave propagation in each homogeneous layer is defined by a displacement field of the form $\exp[j(\mathbf{k} \cdot \mathbf{x} - \omega t)]$, where $\mathbf{k}$ is the wavevector, ω is the angular frequency, and t is the time. Applying continuity of normal displacement at the layer interfaces implies that the components of the wavenumber in the plane of the interfaces (k_2 and k_3) must be equal throughout the structure. This is equivalent to the application of Snell's law. Thus, k_2 and k_3 are the same in all layers, and equal to the components of the incident wave vector. The remaining component of the wave vector in a layer, k_1 is determined by the Christoffel equation, which relates the wave speeds to the elastic properties of the medium, expressed by the stiffness tensor c_{ijkl}:

$$(c_{ijkl}k_j k_k - \rho\omega^2\delta_{il})P_l = 0, \tag{1}$$

where ρ is the density, δ_{il} is the Kronecker delta, and the letters i, j, k, and l, which each will have the value 1, 2, or 3, correspond to the Cartesian coordinate system (x_1, x_2, x_3). This equation also defines the polarization vector components, P_l, for the various wave modes: one pseudo-longitudinal ($p = 1$) and two pseudo-shear ($p = 2, 3$) of different polarizations and speeds. For each mode, two solutions exist for k_1 with the real parts of opposite sign,

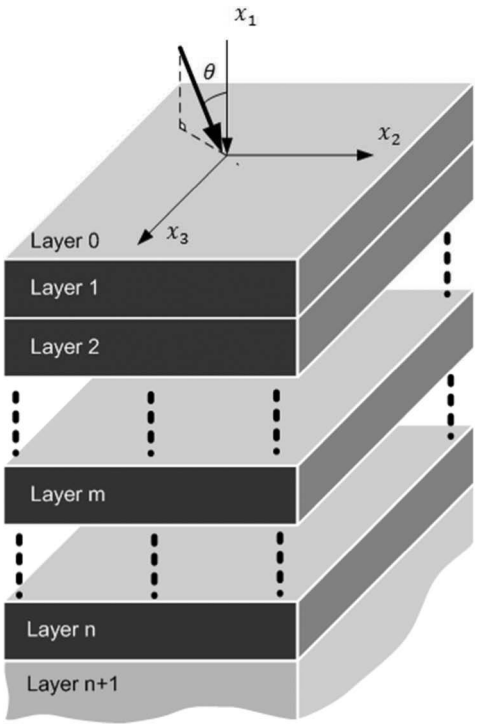

Fig. 1. Configuration of the layered structure modeled by the plane wave model.

one propagating upwards through the layer and the other propagating downwards. Simplification is achieved by the assumption that k_2 and k_3 are real, which is valid if the incident bounding layer is a lossless medium. We will also need to calculate the group velocity which is given (for elastic media, i.e., real stiffness) by

$$v_{gi} = \frac{1}{\rho v} c_{ijkl} P_k P_l \hat{k}_j, \tag{2}$$

where the circumflex denotes the unit vector and v is the phase velocity determined from the Christoffel equation. Thus, the displacement in layer m can be written as a sum over the modes denoted p in the form [10]

$$u_i^m = \sum_{p=1}^{3} [a^{m,p+} P_i^{m,p+} e^{jk_1^{m,p} x_1^m} + a^{m,p-} P_i^{m,p-} e^{-jk_1^{m,p} x_1^m}] \times e^{j(k_2 x_2 + k_3 x_3 - \omega t)}, \tag{3}$$

where $a^{m,p+/-}$ are the amplitudes of the down/up waves, respectively, of mode p in layer m. The coordinate x_1^m is local to layer m, taking the value 0 at the top and d_m at the bottom of the layer.

We wish to determine the reflected and transmitted signals in layer 0 and layer $n + 1$. The solution proceeds as follows. The constitutive equation

$$\sigma_{ij} = c_{ijkl} e_{kl} = \frac{1}{2} c_{ijkl} \left(\frac{\partial u_k}{\partial x_l} + \frac{\partial u_l}{\partial x_k} \right), \tag{4}$$

where e is the strain, can be used for any layer m to relate the stress components on any plane normal to x_1, i.e., σ_{1i}^m, to the local displacement components u_i^m, where $i = 1$, 2, and 3. A layer stiffness matrix S^m is defined, [12] which relates the stress and displacement at the top and bottom of the layer m:

$$\begin{bmatrix} \sigma_{1i}^m(0) \\ \sigma_{1i}^m(d_m) \end{bmatrix} = S^m \cdot \begin{bmatrix} u_i^m(0) \\ u_i^m(d_m) \end{bmatrix} = \begin{bmatrix} S_{11}^m & S_{12}^m \\ S_{21}^m & S_{22}^m \end{bmatrix} \cdot \begin{bmatrix} u_i^m(0) \\ u_i^m(d_m) \end{bmatrix}. \tag{5}$$

The elements of S^m can be derived from (4) with (3). By applying boundary conditions at each interface within the structure (continuity of stress and normal displacement), a combined stiffness matrix S^M that relates stresses and displacements for the top m layers (i.e., layers 1 to m) can be derived

$$\begin{bmatrix} \sigma_{1i}^1(0) \\ \sigma_{1i}^m(d_m) \end{bmatrix} = S^M \cdot \begin{bmatrix} u_i^1(0) \\ u_i^m(d_m) \end{bmatrix} = \begin{bmatrix} S_{11}^M & S_{12}^M \\ S_{21}^M & S_{22}^M \end{bmatrix} \cdot \begin{bmatrix} u_i^1(0) \\ u_i^m(d_m) \end{bmatrix}, \tag{6}$$

where S^M is shown in (7), on next page.

Applying this equation to the whole structure, together with the continuity conditions on stress components at the top and bottom boundaries, results in the solution

$$\begin{bmatrix} \sigma_{1i}^0 \\ \sigma_{1i}^{n+1} \end{bmatrix} = S^N \cdot \begin{bmatrix} u_i^1(0) \\ u_i^n(d_n) \end{bmatrix}, \tag{8}$$

$$S^M = \begin{bmatrix} S_{11}^{M-1} + S_{12}^{M-1}(S_{11}^m - S_{22}^{M-1})^{-1}S_{21}^{M-1} & -S_{12}^{M-1}(S_{11}^m - S_{22}^{M-1})^{-1}S_{12}^m \\ S_{21}^m(S_{11}^m - S_{22}^{M-1})^{-1}S_{21}^{M-1} & S_{22}^m - S_{21}^m(S_{11}^m - S_{22}^{M-1})^{-1}S_{12}^m \end{bmatrix} \tag{7}$$

with the additional continuity condition on normal displacement $u_1^1(0) = u_1^0$ and $u_1^n(d_n) = u_1^{n+1}$, and where S^N is the combined stiffness matrix for the top n layers (i.e., layers 1 to n). Because the incident wave amplitudes are known, and the stress in the bounding layers 0, $n + 1$ can be related to the known incident wave displacements, this equation can be solved for the unknown reflected and transmitted wave amplitudes. The procedure depends on the type of bounding layer. The previous model [12] uses water bounding layers, but here we also consider the case of homogeneous, anisotropic, viscoelastic bounding layers. More detail on this process is given in the subsequent sections.

1) General Case: Anisotropic Bounding Layers: In the general case, assuming incidence from layer 0, with known amplitudes for the incident (downward waves), $a^{0,p+}$, there are three unknown reflected wave amplitudes $a^{0,p-}$, and three unknown transmitted wave amplitudes in layer $n + 1$, $a^{n+1,p+}$. Alternatively, if incidence is from layer $n + 1$, with known incident amplitudes $a^{n+1,p-}$, there are three unknown reflected mode amplitudes $a^{n+1,p+}$ in layer $(n + 1)$ and three unknown transmitted wave amplitudes $a^{0,p-}$ in layer 0. Hence, whether incidence is downward from layer 0, or upward from layer n+1, the unknowns are the upward displacement in layer 0 and the downward displacement in layer n+1.

Because the equation set (8) consists of six equations, only six unknowns can be resolved. In this general case, we have six unknown wave amplitudes, but also the unknown displacement in the plane of the interface in the first and nth layers, $u_2^1(0)$, $u_3^1(0)$, $u_2^n(d_n)$, $u_3^n(d_n)$. To solve this general case, then, an additional boundary condition must be applied, taken here as the no-slip condition on the boundary 0–1 and n–$(n + 1)$. Thus, we apply the condition $u_2^1(0) = u_2^0$, $u_3^1(0) = u_3^0$, and similarly for the bottom interface, $u_2^n(d_n) = u_2^{n+1}$, $u_3^n(d_n) = u_3^{n+1}$. Then, the equation becomes

$$\begin{bmatrix} \sigma_{1i}^0 \\ \sigma_{1i}^{n+1} \end{bmatrix} = S^N \cdot \begin{bmatrix} u_i^0 \\ u_i^{n+1} \end{bmatrix}. \tag{9}$$

The known and unknown parts of the displacement are separated by writing the displacement as a sum of downward- and upward-traveling waves $u_i^m = u_i^{m+} + u_i^{m-}$ so that the unknown terms are u_i^{0-} and $u_i^{(n+1)+}$, and the stress can be written as

$$\sigma_{1i}^m = S^{m+}u_i^{m+} + S^{m-}u_i^{m-}. \tag{10}$$

These new S matrices are not the same as the original layer stiffness matrices, but relate only to upward and downward modes separately. Inserting into (9) and rearranging leads to

$$\begin{bmatrix} S^{0+} - S^{0-} & 0 \\ 0 & S^{(n+1)-} - S^{(n+1)+} \end{bmatrix} \cdot \begin{bmatrix} u_i^{0+} \\ u_i^{(n+1)-} \end{bmatrix} = \begin{bmatrix} S_{11}^N - S^{0-} & S_{12} \\ S_{21}^N & S_{22}^N - S^{(n+1)+} \end{bmatrix} \cdot \begin{bmatrix} u_i^0 \\ u_i^{n+1} \end{bmatrix}, \tag{11}$$

where $S^{0+/-}$ are the up/down matrices defined for layer 0, whereas S^N is the combined stiffness matrix for all layers 1–n.The unknown displacements are on the right hand side of this equation. Terms on the left hand side are known and some may be zero, e.g., if incidence is from layer 0, u_i^{0+} are known, and $u_i^{(n+1)-}$ are zero. The equation can then be solved for the unknown displacements, which can be expressed as reflection and transmission coefficients. The solution for general anisotropic bounding layers has been implemented by the current authors as an extension to the plane wave model implemented by Castaings and LeCrom, which assumes water fluid bounding layers, as considered in the next section.

2) Water Bounding Layers: One special case is relevant for NDT applications, and simplifies the solution for reflected and transmitted amplitudes; that is when the bounding layers (0 and $n + 1$) are water (or other fluid), assumed to be nonviscous and lossless (real wave number). This is the case reported previously [12]–[15]. In this case, no shear wave modes exist in the bounding layers, and the shear stress components are zero. Thus, $a^{0,2+} = a^{0,2-} = a^{0,3+} = a^{0,3-} = 0$, $\sigma_{12}^0 = \sigma_{13}^0 = 0$, and similarly for layer $n + 1$. The incident amplitude of the longitudinal wave mode is assumed to be known, leaving a single reflected longitudinal mode amplitude and a single transmitted longitudinal mode amplitude to be determined, $a^{0,1-}$ and $a^{n+1,1+}$. Because there are only two unknowns in this case, it is possible to avoid the additional application of the no-slip boundary condition, and instead retain the in-plane displacement components in layers 1 and n at the top and bottom interfaces. Hence, we solve (8) with the continuity of normal displacement $u_1^1(0) = u_1^0$ and $u_1^n(d_n) = u_1^{n+1}$, retaining $u_2^1(0)$, $u_3^1(0)$ $u_2^n(d_n)$, and $u_3^n(d_n)$ as unknowns, in addition to the unknown amplitudes $a^{0,1-}$ and $a^{n+1,1+}$ which we require. The polarization of the incident and transmitted longitudinal waves are parallel to the wavevector and of unit amplitude, $\hat{\mathbf{k}}$. Because the bulk modulus for a nonviscous fluid is given by $\rho\omega^2/k^2$, the stress component at the upper interface is given by

$$\sigma_{11}^0 = (j\rho\omega^2/k)[1 + a^{0,1-}]e^{j(k_2x_2 + k_3x_3 - \omega t)}, \tag{12}$$

and similarly for the lower bounding layer, relating to the transmitted wave. This is the only nonzero term of the S^{0+} matrix, and the corresponding term in the S^{0-} matrix has the opposite sign. Taking the instance of the top bounding layer being water, the solution can be obtained from (11) by replacing u_i^{0-} by $(u_1^{0-}, u_2^1(0), u_3^1(0))$ and u_i^{0+} by $(u_i^{0+}, 0, 0)$. This is possible because of the simple form of the stress terms in a nonviscous fluid. The solution may also be obtained more directly from (8).

B. Angular Spectrum Method

Having obtained the response of the anisotropic multilayered structure to monochromatic plane waves with a given incident wave vector $\mathbf{k}$, its response to finite beams, such as might be expected from transducer array elements, is now constructed using the angular spectrum method. The method uses a Fourier decomposition to relate spatial and wavevector variation, thus permitting finite beams to be modeled by summing over different incident wavevectors with different amplitudes, relating to the directivity of the transducer elements. Because an incident wave of wavevector $\mathbf{k}$ of unit amplitude at the top bounding layer results in a reflected wave of wavevector $\mathbf{k}^-$ (which has the k_1 component reversed), the response at the top bounding layer is denoted $G_{\mathrm{TT}}(\mathbf{k}, \mathbf{k}^-, \omega)$, which corresponds to the wave mode amplitudes obtained in the previous section (Section II-A). The transducer elements are characterized by a directivity function, D. The angular spectrum model then defines the amplitude of the receiving array element response at position $\mathbf{x}$ and frequency ω by

$$\mathbf{F}(\mathbf{x}, \omega) = \int \hat{\mathbf{k}}^- D_{\mathrm{t}}(\mathbf{k}) D_{\mathrm{r}}(\mathbf{k}) G_{\mathrm{TT}}(\mathbf{k}, \mathbf{k}^-, \omega) e^{j\mathbf{k}^- \cdot \mathbf{x}} \mathrm{d}k_1 \mathrm{d}k_2 \mathrm{d}k_3. \tag{13}$$

The value of k_1 is fixed by k_2 and k_3 and the wavespeed in water, so that the integration is only over two components. The subscripts t and r denote transmitter and receiver, respectively.

For a 1-D linear array, in which the array elements are long in the x_3 direction, each element can be considered as a modified line source, with directivity pattern

$$D_{\mathrm{t}}(\hat{\mathbf{k}}) = \mathrm{sinc}\left(\frac{\pi W \sin\theta}{\lambda}\right), \tag{14}$$

where the angle $\theta = \tan^{-1}(k_2/k_1)$, λ is the wavelength (in the bounding layer which is in contact with the array element), and W is the width of the element. This configuration corresponds to the constraint $k_3 = 0$ (Fig. 1).

This general formulation of the angular spectrum method thus allows any finite beam to be analyzed using the plane wave model as the kernel response. The final step in obtaining the time-domain response for the transducer array is to apply the Fourier transform to the frequency-domain response, multiplied by the frequency response of the transducer elements, $H(\omega)$, in the usual way

$$f(\mathbf{x}, t) = \int H_{\mathrm{t}}(\omega) H_{\mathrm{r}}(\omega) \mathbf{F}_1(\mathbf{x}, \omega) e^{-j\omega t} \mathrm{d}\omega, \tag{15}$$

where $\mathbf{F}_1(\mathbf{x},\omega)$ is the component of displacement normal to the transducer element i.e., in the direction $\hat{\mathbf{x}}_1$.

The simulations are greatly simplified by the assumption that all array elements are identical, both in directivity pattern, and in frequency response, as demonstrated by [32]. Using the angular spectrum method, and the plane wave model, it is possible to simulate the full data set of received signals for a transducer array interrogating both homogeneous and inhomogeneous material such as a composite laminate.

C. Equivalent Homogeneous Properties

At low frequency (long wavelength), the response of the layered structure approaches that of a homogeneous medium, whose properties are termed the equivalent homogeneous properties (EHP). In this frequency region, the reflections from individual layer boundaries are not seen, and propagation appears to be undisturbed by the interfaces. The equivalent homogeneous properties for a composite structure can be estimated and used to model the structure as a single layer of homogeneous material. The total focusing algorithm used for ultrasonic array imaging adopts such an assumption, attributing travel time delays between locations in the specimen and array elements based on uniform specimen properties. Various methods have been reported in the literature to obtain the equivalent homogeneous properties, including inversion of time-of-flight measurements in composites at a variety of propagation directions, using the Christoffel equation to determine the stiffness properties [33]–[37]. Alternatively, averaging techniques can be used to estimate stiffness matrix elements, such as those developed in the context of seismological studies by Postma [38] and Backus [30], and adopted in the composites literature, for example [31].

We have used the Backus method for homogenization, which relies on the assumption of constant or slowly varying normal stress and in-plane strain components. These components are continuous at each layer boundary (stress continuity and no-slip condition), and according to classical lamination theory, are also constant through each layer. Thus the components, σ_{1j}, e_{22}, e_{33}, and e_{23} are all constant (Backus assumes only that they are slowly varying) through the thickness of the structure. The constitutive equation (4) is rearranged such that the constant terms are on the right-hand side multiplying the stiffness terms, and the varying stress and strain components are on the left-hand side. A thickness-weighted averaging through the thickness direction, then leads to the averaged stiffness matrix properties. Rearrangement back to the constitutive equation format allows the averaged stiffness values to be identified. Using Voigt notation, the stiffness matrix is defined as a set of submatrices:

$$c = \begin{pmatrix} E_{11} & D_{11} & D_{12} & D_{13} & E_{12} & E_{13} \\ A_{11} & B_{11} & B_{12} & B_{13} & A_{12} & A_{13} \\ A_{21} & B_{21} & B_{22} & B_{23} & A_{22} & A_{23} \\ A_{31} & B_{31} & B_{32} & B_{33} & A_{32} & A_{33} \\ E_{21} & D_{21} & D_{22} & D_{23} & E_{22} & E_{23} \\ E_{31} & D_{31} & D_{32} & D_{33} & E_{32} & E_{33} \end{pmatrix}, \quad (16)$$

with $D = A^T$. The equivalent homogeneous properties are obtained by averaging combinations of the submatrices as follows

$$A^* = \langle AE^{-1}\rangle\langle E^{-1}\rangle^{-1} \quad (17)$$

$$B^* = \langle AE^{-1}\rangle\langle E^{-1}\rangle^{-1}\langle E^{-1}D\rangle + \langle B - AE^{-1}D\rangle \quad (18)$$

$$E^* = \langle E^{-1}\rangle^{-1} \quad (19)$$

$$D^* = \langle E^{-1}\rangle^{-1}\langle E^{-1}D\rangle = A^{*T}. \quad (20)$$

This set of equations can be used to determine the equivalent homogeneous properties (stiffness) of a complete composite sample or part of it, and thus to simulate the ultrasonic propagation at low frequency. In this work, the EHP have been used for the whole composite to estimate values of group velocity for imaging purposes (see Section II-F), and also as part of a model of a defect embedded in composite which is reported in the next section.

D. Scattering From an SDH

To model the transducer array signals for an SDH embedded in a composite material, it is first necessary to consider the scattering from such a hole in a homogeneous medium, and then to combine this scattered field with the propagation through the layered structure. The first of these steps follows the findings of Huang *et al.* [39]–[40] who used the Kirchhoff approximation to study the scattering of elastic waves from SDHs in homogeneous anisotropic materials in pulse–echo mode (i.e., backward scatter). They demonstrated that the leading edge received scattered signal was identical to that from the same SDH in an isotropic medium which has the properties of the original medium at the corresponding angle of incidence. This implies that the dominant scattered signal can be successfully modeled using isotropic embedding material, but choosing the properties of the isotropic material appropriate to the angle of incidence.

The scattering from the SDH was then modeled using the separation of variable results from Lopez-Sanchez *et al.* [23] for an isotropic embedding medium with a planar longitudinal incident wave of unit amplitude in displacement, giving a scattered longitudinal-mode amplitude of

$$\Gamma^{l-l}(\alpha) = \left(\frac{2i}{\pi k_l}\right)^{1/2} \sum_{q=0}^{\infty} (2 - \delta_{0q})(k_l b) A_q \cos(q\alpha) \quad (21)$$

at an angle α between the incident and scattered wavevectors. Here, the longitudinal and shear wavenumbers of the isotropic embedding medium are denoted k_l and k_s, respectively, b is the radius of the SDH, δ_{0q} is the Kronecker delta, and the coefficients A_q are

$$A_q = \left(\frac{i}{2k_l b}\right)\left[1 + \frac{C_q^{(2)}(k_l b)C_q^{(1)}(k_s b) - D_q^{(2)}(k_l b)D_q^{(1)}(k_s b)}{C_q^{(1)}(k_l b)C_q^{(1)}(k_s b) - D_q^{(1)}(k_l b)D_q^{(1)}(k_s b)}\right], \quad (22)$$

where

$$C_q^{(i)}(x) = (q^2 + q - (k_s b)^2/2)H_q^{(i)}(x) - xH_{q-1}^{(i)}(x) \quad (23)$$

$$D_q^{(i)}(x) = (q^2 + q)H_q^{(i)}(x) - qxH_{q-1}^{(i)}(x), \quad (24)$$

and $H_q^{(i)}$ denotes the Hankel function of the first and second kind, respectively, for $i = 1, 2$. For incident plane wave direction $\hat{\mathbf{k}}$ and scattered direction $\hat{\mathbf{k}}'$, the scattering angle is given by $\alpha = \theta' - \theta$, where θ and θ' are the angle of the incident and scattered waves with the x_1-axis, respectively.

E. SDH Embedded in Composite

To model the ultrasonic signals for an SDH in a composite material, we have combined the scattered radiation profile for an SDH with the model for transducer array signals in layered composites. This has been achieved by treating the SDH as a source or transmitter, with a directivity given by the scattered field reported in the previous section. This is combined with the response of the layered structure using the plane wave model, in two stages—from the top to the bottom (SDH location), and from the SDH location to the top. Fig. 2 shows the configuration adopted in the model for the embedded SDH in the multilayer structure [Fig. 2(a)]. The region containing the defect (SDH) is modeled as a single semi-infinite homogeneous medium [see Fig. 2(b)], which acts as the lower bounding layer of the structure; its properties are obtained using the equivalent homogeneous properties defined in Section II-C. The top of the lower bounding layer is located some distance above the SDH, because the scattering coefficients (Section II-D) define the far-field response. The upper bounding layer is water.

For an incident plane wave of unit amplitude and wavevector $\mathbf{k}$ from the top bounding layer, the transmitted wave in the lower bounding layer has wavevector $\mathbf{k}^i$ which is incident at the defect. Although the polarization vector in the anisotropic bounding region is not parallel to the wavevector, the incident direction for the scattering at the defect is taken as $\mathbf{k}^i$ because we are using an isotropic embedding medium approximation for the scattering. The field scattered by the defect in a direction $\mathbf{k}^o$ (in the lower bounding layer) is transmitted through the layered structure to the upper bounding layer, emerging with wavevector $\mathbf{k}'$. Thus the response for incident wavevector $\mathbf{k}$ and output wavevector $\mathbf{k}'$ can be written

$$G_{\mathrm{TT}}(\mathbf{k}, \mathbf{k}', \omega) = G_{\mathrm{TB}}(\mathbf{k}, \mathbf{k}^i, \omega)\Gamma(\mathbf{k}^i, \mathbf{k}^o)G_{\mathrm{BT}}(\mathbf{k}^o, \mathbf{k}', \omega), \quad (25)$$

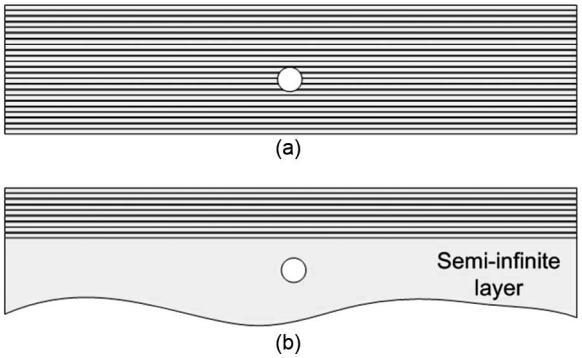

Fig. 2. Configuration for modeling a side-drilled hole in a layered composite material. (a) Side-drilled hole (SDH) embedded in the multilayer structure and (b) model representation of the SDH in the multilayer structure.

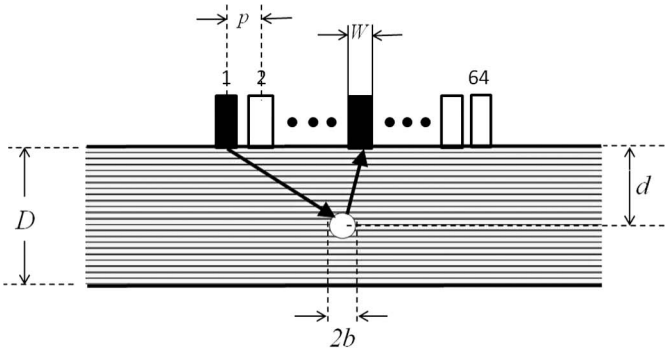

Fig. 3. Configuration for experiment and simulation showing 1-D linear ultrasonic transducer array with homogenous or composite material, and an embedded defect.

where the subscripts TB, BT, and TT on the response functions denote top-to-bottom, bottom-to-top, and top-to-top layer responses, respectively. The plane wave responses are derived from the results in Section II-A for the appropriate bounding layer properties. The angles used to calculate the scattering function are defined by $\theta = \tan^{-1}(k_2/k_1)$. The angular spectrum method can then be applied to this system response for all combinations of input and output wavevectors, to determine the overall system response, thus

$$\mathbf{F}(\mathbf{x},\omega) = \iint \hat{\mathbf{k}}' D_{\mathrm{t}}(\mathbf{k}) G_{\mathrm{TT}}(\mathbf{k},\mathbf{k}',\omega) D_{\mathrm{r}}(\mathbf{k}') e^{j(\mathbf{k}+\mathbf{k}')\cdot\mathbf{x}} \mathrm{d}k_2' \mathrm{d}k_2. \tag{26}$$

Integration is now only over the second component of the wavevectors, because $k_3 = 0$ using a 1-D linear array.

Whereas in the absence of a defect, the number of calculations in the model for the system response scales with $N_k \log N_k$ (the number of k-vectors chosen for the Fourier transform), here (with defect) it scales with $N_k^2 \log N_k$. Thus, the defect-in-composite model is likely to be considerably slower than the defect-free model. To achieve a more efficient calculation, an alternative, approximate model was constructed. In this case, the angular spectrum is applied to the top-to-bottom response to obtain an effective amplitude at the defect. The incident wave at the defect is assumed to be planar in the direction of the straight path between transmitter and defect, (Fig. 3) using the component of the amplitude in that direction. Similarly the bottom-to-top responses for all wave directions from the bottom layer are combined in the angular spectrum method, to determine the amplitude in the direction of the straight path between defect and receiver. These two response amplitudes are combined with the scattering function for the defect, taking the two straight-path directions to define the scattering angles. Because two sets of angular spectrum calculations are carried out, the model scales with $N_k \log N_k$, offering a potentially considerable decrease in computation time. The relevant equations for the consecutive angular spectrum calculations and the combination with the scattering function are

$$\mathbf{F}_{\mathrm{TB}}(\mathbf{x},\omega) = \int \hat{\mathbf{k}}^i D_{\mathrm{t}}(\mathbf{k}) G_{\mathrm{TB}}(\mathbf{k},\mathbf{k}^i,\omega) e^{j\mathbf{k}\cdot\mathbf{x}} \mathrm{d}k_2 \tag{27}$$

$$\mathbf{F}_{\mathrm{BT}}(\mathbf{x},\omega) = \int \hat{\mathbf{k}}' G_{\mathrm{BT}}(\mathbf{k}^o,\mathbf{k}',\omega) D_{\mathrm{r}}(\mathbf{k}') e^{j\mathbf{k}^o\cdot\mathbf{x}} \mathrm{d}k_2^o \tag{28}$$

$$\mathbf{F}(\mathbf{x},\omega) = \hat{\mathbf{k}}_{\mathrm{DR}} F_{\mathrm{TB}} \Gamma(\hat{\mathbf{k}}_{\mathrm{TD}},\hat{\mathbf{k}}_{\mathrm{DR}}) F_{\mathrm{BT}}, \tag{29}$$

where F_{TB} and F_{BT} are the components of the displacements $\mathbf{F}_{\mathrm{TB}}$ and $\mathbf{F}_{\mathrm{BT}}$ in the direction of the straight path from transmitter to defect and defect to receiver, respectively. The displacement amplitudes are all as a proportion of the incident (unit) amplitude, and are therefore dimensionless.

These models for the response of a defect in a layered structure are, to our knowledge, novel. They permit the investigation of improved imaging algorithms for defect detection in composite materials.

F. Image Generation From Array Signal Data Set

Thus far, we have reported models which can simulate the data set obtained using a transducer array in FMC mode (in which each element acts consecutively as transmitter, while recording the received signals on all elements). In post-processing such data to produce an image of the cross-section of the material, the time delays between each array element pair to each point on a grid in the material must be calculated. By summing the received signals with the appropriate time delays, the signal received from any particular point in the material can be determined, resulting in an image of the material. The method relies on the response of the structure being similar to an equivalent homogeneous medium, in which the travel times are related to the angle-dependent group velocity in the material.

An empirical way to measure the anisotropic group velocity in composite is to use the arrival times of the back wall echoes in either simulated or experimental FMC signals. This method is time consuming for simulation and not always practical experimentally (for example, if the specimen does not have a flat back wall parallel to the inspection surface). For both simulations and experiments, the whole FMC data must be measured first and

TABLE I. STIFFNESS AND DENSITY OF MATERIALS.

Property	Aluminum [41]	Homogenized fiber-resin [42]	Resin [43]
C_{11}, C_{22} (GPa)	110	$14\ (1 + 0.01j)$	$5 + 0.25j$
C_{33} (GPa)	110	$125\ (1 + 0.01j)$	$5 + 0.25j$
C_{12}, C_{23} (GPa)	60	$6.5\ (1 + 0.01j)$	$2 + 0.1j$
C_{13} (GPa)	60	$8\ (1 + 0.01j)$	$2 + 0.1j$
C_{44}, C_{55} (GPa)	25	$5.5\ (1 + 0.01j)$	$1.5 + 0.08j$
C_{66} (GPa)	25	$3.75\ (1 + 0.01j)$	$1.5 + 0.08j$
ρ (kg·m^{-3})	2780	1500	1100

then used to calculate the group velocities. An alternative, simple method is to use the equivalent homogeneous properties of the whole composite (see Section II-C) to obtain the relevant group velocities using (2), and hence time delays. All images and post-processing of simulated or experimental FMC data have been processed in this way in this work.

The array aperture used to form the image at each point is chosen so that only rays that propagate within a specified angular range are considered. In other words, the ratio of the depth to the aperture (i.e., f-number) is constant so that the angle subtended by the aperture at each image point is kept constant.

G. SNR for SDH Response

In defect detection for nondestructive testing, one key parameter is the SNR for a defect. In the configuration under consideration here, the signal relates to the response from the defect (a SDH), and the noise is in fact structural noise, resulting from reflections at the layer interfaces. The SNR has been calculated from the images produced using the TFM algorithm, based on the group velocities from the EHP, obtained from simulated FMC data. Two FMC data sets were simulated: (a) without the SDH, using the full layered composite structure and (b) with the SDH, using the models described in Sections II-D and II-E. The latter results, (b) are denoted signal FMC and the former, (a) are used to represent noise FMC (unwanted signal resulting from structural effects). Both data sets are transformed using TFM to produce a corresponding amplitude image. The *signal* in the SNR is defined as peak amplitude in the signal image from (b) caused by the defect, and the *noise* as the root mean square signal in the noise image obtained from (a) in the immediate vicinity of the defect location (with the defect signal absent). The region was defined as a rectangular section of depth 1 cm and width 2 cm centered on the defect location.

III. MATERIALS AND METHODS

The configuration of the system is shown in Fig. 3, with the transducer array in contact with the material through a coupling gel. Two arrays have been used in experiment and simulation: array A has a center-frequency of 5 MHz, pitch $p = 0.63$ mm, and element width $W = 0.53$ mm, whereas array B has 2.5 MHz center frequency, $p = 0.5$ mm, and $W = 0.35$ mm. Further experimental details are given in [3]. Simulations were carried out in Matlab.

Two materials have been used in simulation and experiment: aluminum (a homogeneous, near-isotropic material), and a carbon-fiber reinforced composite (CFRC). The stiffness and density for the materials are given in Table I. For aluminum, the material is assumed to be purely elastic, implying that the attenuation is zero [41]. A 30-mm-thick plate of aluminum was tested using the 5-MHz array.

Two samples of CFRC have been used; these were supplied by one of the project partners, who also provided details of the lay-up and ply thickness. For the purposes of the model, the CFRC plate is assumed to consist of unidirectional, homogeneous, anisotropic layers of fiber/resin bounded by homogeneous isotropic resin layers. The stiffness matrices for the layers were not provided and it was not possible to measure them directly. Instead, values for a typical fiber/resin material (with fiber orientation of 0°) were taken from [42] and for resin layers from [43]; these are listed in Table I. In this case, the stiffness values are complex, indicating a viscoelastic component which causes attenuation of the ultrasonic signals. Sample A is 16 mm thick, having 128 plies, each 120 μm thick, with 5-μm resin layers. Sample B is 19 mm thick, with 82 plies of 225 μm thickness and 5 μm resin thickness. In this sample, a 1.5-mm-diameter SDH is located at depth $d = 10$ mm (to its center) from the top surface in part of the sample. For both samples, the ply lay-up was taken as 0°/45°/−45°/90°, in a repeated sequence and tests and simulation were carried out with the 2.5-MHz transducer array, this frequency having been used successfully in experimental studies on such materials [3]. These two samples provide validation with different layer thicknesses and with or without a defect. For modeling the defect response, the top of the lower bounding layer (the equivalent homogeneous medium) is located at a distance of 2 mm from the top of the hole. All experiments were carried out with the transducer array in contact with the material using a gel couplant. It is assumed that the gel does not support shear tractions, hence the array elements are assumed to apply normal stresses only. This is consistent with the boundary conditions for a water layer given in Section II-A; hence, simulations assume a water bound-

ing region to the material to represent the gel couplant. The response of a component to a finite-width gel-coupled array element can be obtained by superposition of the responses to incident planar longitudinal waves in water over all possible angles, as indicated by the integral in (13), the finite width of the element being accounted for in the $D(\mathbf{k})$ factors.

IV. Results

A. Array Element Response

To characterize the frequency response for the transducer array elements, $H(\omega)$ (see Section II-B), the back wall echo was obtained, with element 1 of the array acting as both transmitter and receiver. The results for the aluminum plate (with the 5-MHz array) and the CFRC sample A with the 2.5-MHz array are shown in Fig. 4. This echo includes the combination of the transmission and reception responses of the transducer and of the propagation path to and from the back wall of the specimen. The transducer responses were obtained from echoes off a flat metal surface immersed in water; they are not shown here because they were similar to the responses given in Fig. 4.

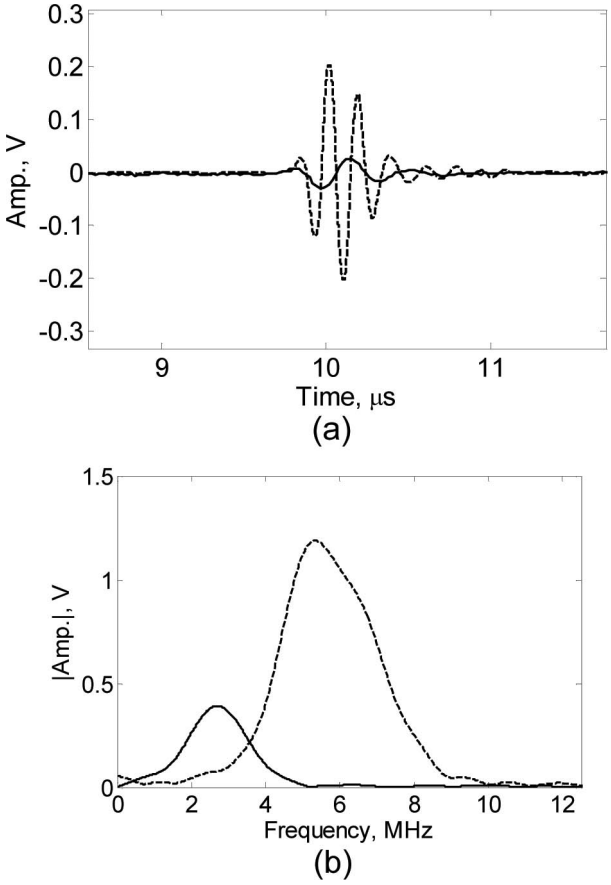

Fig. 4. Back wall echo signal, using transducer array element 1 as both transmitter and receiver (normal incidence). (a) time domain and (b) frequency domain, for aluminum plate (dashed line) and carbon-fiber reinforced composite (CFRC) plate A (solid line).

B. FMC for Homogeneous Material and Layered Composite

Simulations of a set of transducer array signals based on the model described in Sections II-A and II-B have been carried out for both aluminum and CFRC samples. These have been compared with experimental measurements to establish the validity of the models. Use of an isotropic material (aluminum) allows the model to be validated for a simple case, confirming the correct mode conversion and arrival times, before validating with an anisotropic layered material (composite samples) in which the wave propagation is much more complex. For the aluminum plate, with a 5-MHz array, the simulated and measured time-domain signals are shown in Fig. 5 for transmission on element 1, and reception at several selected array elements.

In the experimental data [as shown in Fig. 5(a)], some electrical breakthrough can be seen near the origin of the time-axis on all receiving elements; this is absent in the simulated data [Fig. 5(b)]. However, the reflection from the front face of the sample can be seen in the simulated data for element 1 in Fig. 5(b) at a very short time after transmission. The next arrival received by element 1 is at around 10 μs and corresponds to the first longitudinal mode echo from the back wall. For the other receiving elements, the corresponding signal arrives later the more distant the element is from element 1. Its amplitude and arrival time is predicted accurately by the model. The second, small-amplitude signal, arriving between 15 and 17 μs is a slower signal, which has undergone mode conversion at either top or bottom surface. It corresponds to a combination of a longitudinal mode converted to shear at the back wall, and then back to longitudinal at the top surface, and a shear mode produced at the top surface, converted to a longitudinal mode at the back wall. Because mode conversion does not occur for normal incidence, this signal is absent from the first element response. Waves transmitted from element 1 at angles away from the normal, because of its finite size, are capable of mode conversion, but are received primarily at other elements except for those angles extremely close to the normal which could be received at the same element. The contribution from these paths is likely to be very small, hence mode conversion is not seen when transmitting and receiving on the same element. However, the amplitude of the mode-converted signal increases as the incident angle increases (i.e., for receiving elements further from element 1). The final received signal shown is the second longitudinal mode back wall echo. Agreement between simulation and experiment is excellent for this homogeneous material.

Simulated and experimental array data are shown in Fig. 6 for the CFRC sample A using the 2.5-MHz center frequency array. In this case, there is a significant reduction in the amplitude of the back wall echoes arriving at around 11 μs, compared with the aluminum case (see Fig. 4). For CFRC, we have shown only up to receiver number 20, because those signals received further from the trans-

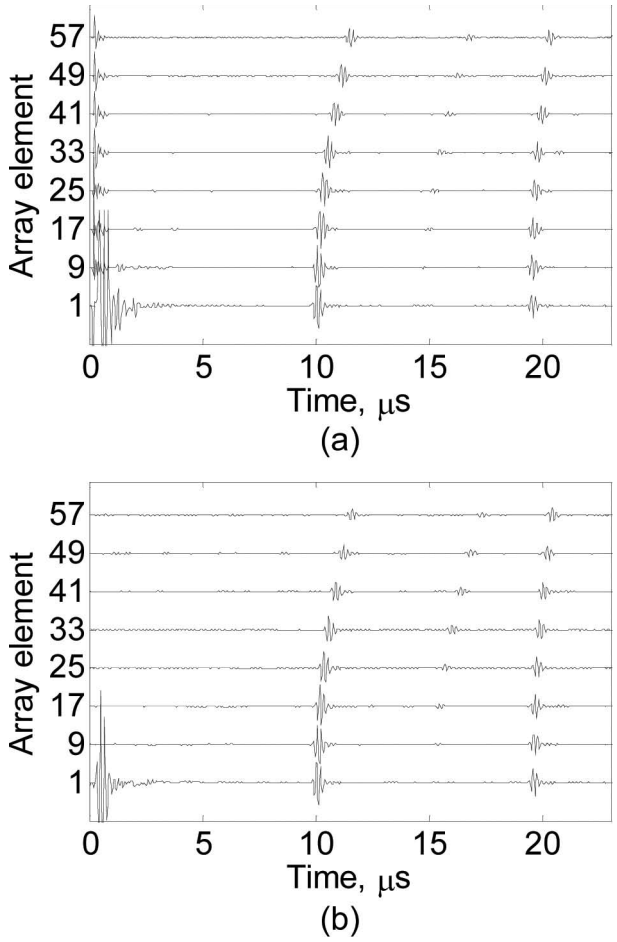

Fig. 5. Ultrasonic transducer array signals received on various array elements with element 1 as transmitter, for a 5-MHz center frequency array with a 30-mm aluminum plate: (a) experiment and (b) simulation.

mitter have such small amplitude. These losses are due to damping in the viscoelastic matrix of the composite, and to diffraction from the layer interfaces. The reflected signals from the layer interfaces can be clearly seen in the region 1 to 6 μs in both experimental and simulated data; these are absent in the aluminum case. The amplitude and arrival time of both back wall echoes and these structural signals are simulated well by the model. Any discrepancies can be attributed to the uncertainty in physical properties of the materials.

C. Group Velocity

The effective angle-dependent group velocity in the materials has been determined from the first arrival times of the back wall echo in the experimental data. A similar method has been applied to the simulated FMC data. Results for composite sample A with the 2.5-MHz transducer array are shown in Fig. 7. For aluminum, the propagation speed does not vary with angle, and the velocity obtained from experimental data was 6295.4 ± 18.8 m/s compared with a value of 6290 m/s calculated from the stiffness and density which were used in the model (Table I). For composite, the group velocity has also been calculated from the equivalent homogeneous properties of the sample (see Section II-C), as shown in Fig. 7.

The results show excellent agreement for the longitudinal mode between experiment and simulation, and also with the EHP estimate of the group velocity. The variation in speed is, in fact, very small up to around 20°, so that a simple isotropic time-delay algorithm would work satisfactorily in this range. Experimental data are available only up to 40° because of the attenuation of the back wall signal and array size constraints. The agreement with the EHP results demonstrates that the simple EHP calculation could be used to calculate the appropriate angle-dependent velocity (theoretically up to 90°) for obtaining time-delay laws for the imaging algorithms. This avoids the time-consuming experimental determination, or corresponding computational modeling. Fig. 7 also shows calculations for the two pseudo-shear mode group velocities using EHP, values that cannot be calculated using experimental FMC data because of their higher losses.

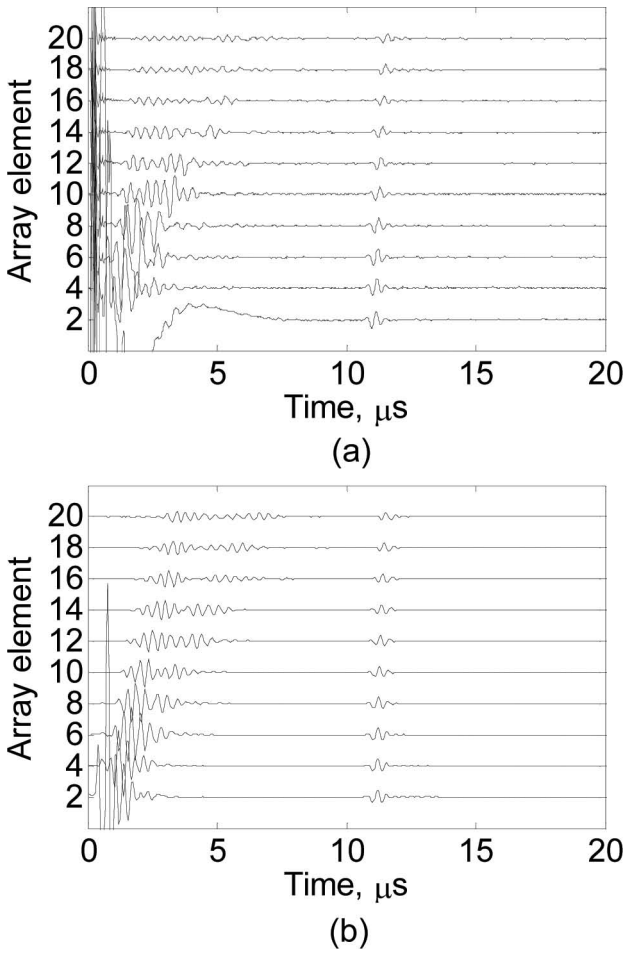

Fig. 6. Ultrasonic transducer array signals received on various array elements with element 1 as transmitter, for a 2.5-MHz center frequency array with a 16-mm carbon-fiber reinforced composite (CFRC) sample with no defect (sample A): (a) experiment and (b) simulation.

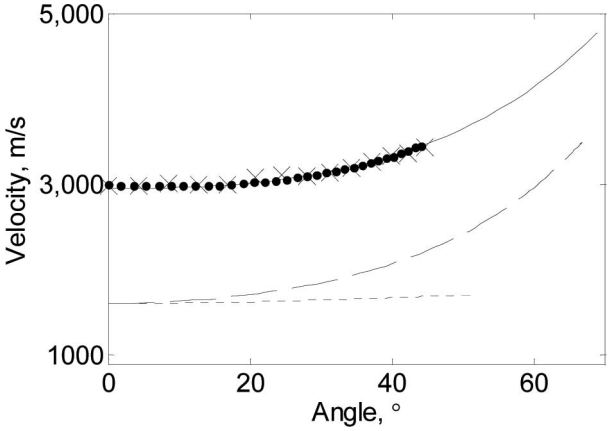

Fig. 7. Group velocity as a function of propagation angle for fiber/resin composite. Estimation from first arrival times of the back wall echo using experimental (black dots) and simulated data (crosses) are compared with the results from the equivalent homogeneous properties (solid lines) for the pseudo-longitudinal mode. The dashed and dotted lines show the group velocity calculated from the equivalent homogeneous properties for the two pseudo-shear modes.

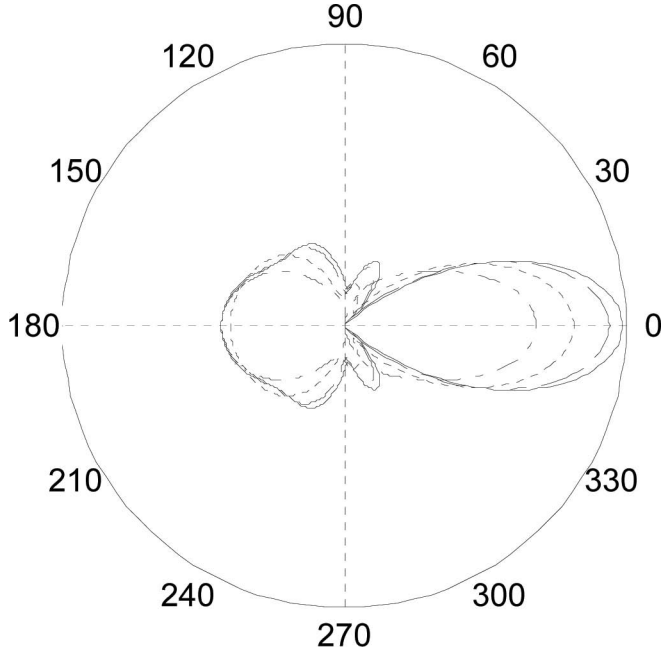

Fig. 8. Scattering amplitude as a function of angle for longitudinal-longitudinal scattered fields for a 1.5-mm-diameter side-drilled hole (SDH) in an isotropic medium in which the wavenumber is the same as that at the given incident angle in the equivalent homogeneous medium for the composite. The plots have been rotated such that the plotted angle is relative to the incident direction, which is along the 0° axis in each case. The figure shows scattering amplitudes for incident propagation angles of 0° (solid line), 20° (dashed line), 40° (dotted line), and 60° (dash-dot line). The outer circle is an amplitude of 1.5 $m^{0.5}$.

D. Defect in Composite

The scattered field from a 1.5-mm-diameter cylindrical hole in an isotropic medium is shown in Fig. 8, see Section II-D. The results are shown for different wave-numbers in the isotropic embedding medium (21), corresponding to the wave-numbers in the anisotropic, equivalent homogeneous medium of the composite, at the appropriate incident angle. Very little change in scattering pattern is seen up to 20° incident angle, consistent with the group velocity calculation. This field pattern is used as a directivity function associated with the SDH when it acts as a source in modeling (Section II-E).

We have simulated the response of the SDH defect in composite sample B using the two models described in Section II-E. A comparison of the time-domain response obtained using the two models is shown in Fig. 9 for a particular transmitter–receiver pair. The agreement between the two models is very good, both in phase and amplitude of the signals, although the approximate method gives a slightly reduced amplitude. The difference between them is strongly dependent on the nature of the scattering function and its degree of anisotropy, and on the angle between transmitting and receiving elements at the defect. However, these results demonstrate that the simpler, more efficient model makes a very good estimate of the response of the defect in the layered composite, and could be applied where greater speed of computation is required. For the investigations that follow, the results from the full angular spectrum method [(25) and (26)] were used.

To assess the accuracy of the TFM imaging algorithms, we have produced images from these simulated data sets and estimated the SNR for the defect as described in Sections II-F and II-G. The imaging algorithm was based on the group velocity determined from the equivalent homogeneous properties for the composite (Section II-C). The two images are shown in Fig. 10; the first shows the "noise" arising from reflections at layer boundaries, whereas the second shows the "signal" received from the defect itself. The image algorithm used all available simulated array data, to the full aperture of the array. The two images were normalized using the back wall echo in the noise

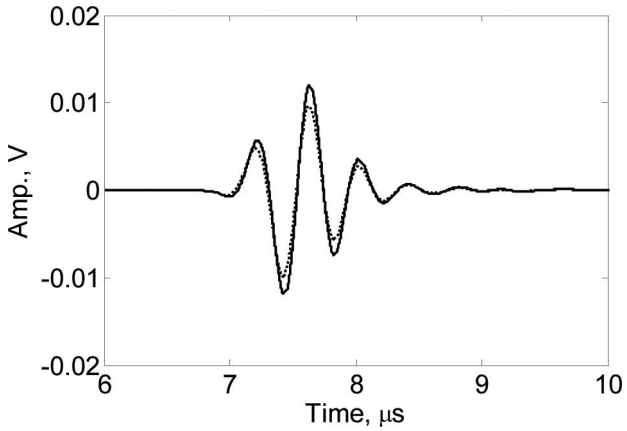

Fig. 9. Ultrasonic transducer array signals for transmission on element 27, and reception on element 42, corresponding to a transmitted angle of 11.3° and receiving angle of 24.2° to the normal. The results were calculated from the full angular spectrum model (solid line), [(25) and (26)] and from the approximated model (dotted line), [(27)–(29)]. The defect is a side-drilled hole of diameter 1.5 mm embedded in composite sample B at a depth of 10 mm.

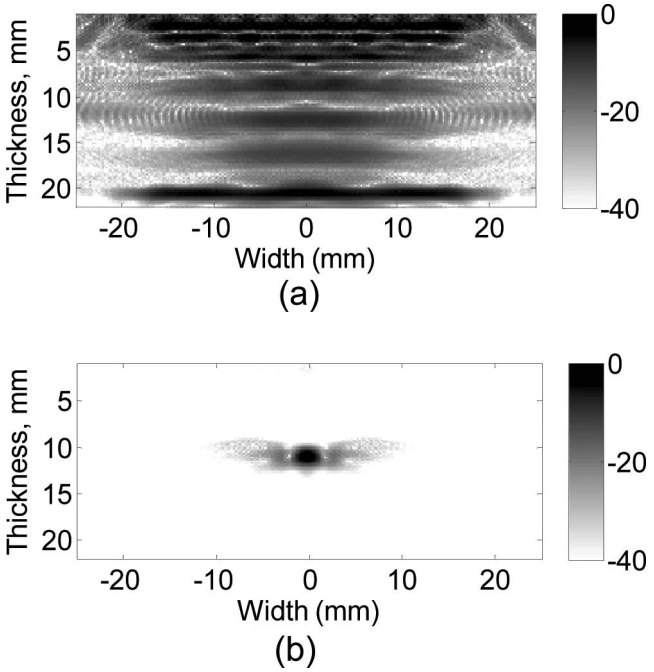

Fig. 10. Images from simulated array data for a 1.5-mm-diameter side-drilled hole at a depth of 10 mm in composite sample B, using the 2.5-MHz center frequency array. (a) the "noise" image: composite with no defect, and (b) the "signal" image: defect only (see Section II-G).

(defect-free) image (a). The defect, instead of appearing circular, is spread out over a much larger distance.

To investigate the effect of using an aperture angle limit in the imaging algorithm, as proposed experimentally in [3], the SNR has been calculated (Section II-G) from the simulated images, using different aperture angle limits. The results are shown in Fig. 11. As the maximum aperture angle increases up to ∼10°, the additional information included in the image improves the SNR. However, the SNR has a peak value at a particular angle, above which an increase in the maximum aperture angle degrades the SNR of the defect in the image; this is due to the contribution of structural noise (from the layer interfaces), which adds coherently. In contrast, the SNR in a homogeneous material such as aluminum has no maximum, because the noise adds incoherently, so increasing the maximum aperture angle systematically improves the SNR. The simulated SNR data support the conclusion, observed experimentally, that use of an aperture angle limit leads to an improvement in image quality for composites [3].

V. Conclusion

Simulation of transducer array signals for composite materials is a potentially valuable tool for improving imaging algorithms. The models reported in this paper allow the simulation of full matrix array data for homogeneous or anisotropic layered composite materials such as CFRC. This has been achieved by the combination of a plane wave model to obtain the response to plane incident waves, and the angular spectrum method to simulate finite beams from transducer elements. In addition, a method for obtaining the equivalent homogeneous properties of a composite has been exploited to estimate the angle-dependent group velocity through the composite, which can be used in imaging algorithms for calculating delay laws. In a novel development, the scattering from an SDH defect has been introduced into the model of the layered composite system, to simulate the response of a defect in composite.

A comparison between the simulated and experimental transducer array data shows excellent agreement, both in time-domain responses, and in the effective angle-dependent group velocity. Having validated the model in this way, two improvements to imaging algorithms which have been recently proposed [3] have been assessed. The first is the use of an angle-dependent velocity to calculate delay laws, which has been shown experimentally to improve image quality [3]. Our results have shown agreement between the velocity obtained from simulated and experimental data using back wall echoes, and we have also validated an analytical method for obtaining those velocities from the equivalent homogeneous properties. This method allows the calculation of angle-dependent velocity for use in imaging algorithms without resort to a complex computational model, or reliance on back wall echo experimental data. The second algorithm improvement is the use of a limited aperture angle, which has been shown experimentally to improve the SNR for a defect [3]. In the current work, that conclusion is supported by the finding of a maximum in the SNR as a function of the maximum aperture angle, based on simulations of the defect in composite. It is believed that this is due to the coherence of structural noise, i.e., signals from the reflections at layer interfaces, which does not decrease as the aperture increases (as it would for incoherent noise from a homogeneous material).

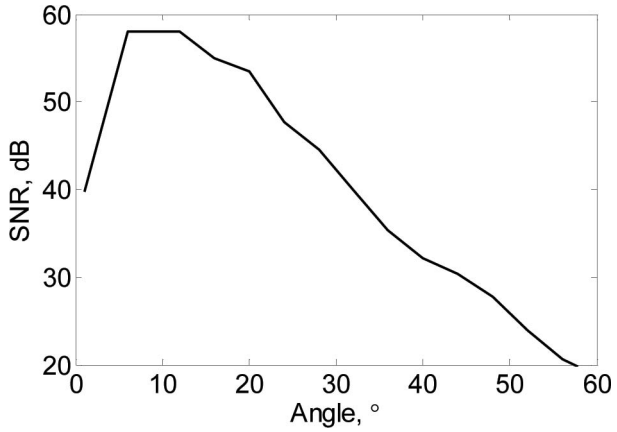

Fig. 11. Simulated SNR for simulated data for a 1.5-mm side-drilled hole (SDH) in composite sample B, as a function of aperture angle limit using the 2.5-MHz array.

Acknowledgments

We are grateful to M. Castaings and B. LeCrom from the University of Bordeaux 1, who wrote the Matlab code for the plane wave model with water bounding layers described in Section II-A.

References

[1] C. Holmes, B. W. Drinkwater, and P. D. Wilcox, "Post-processing of the full matrix of ultrasonic transmit-receive array data for non-destructive evaluation," *NDT Int.*, vol. 38, pp. 701–711, Dec. 2005.

[2] B. W. Drinkwater and P. D. Wilcox, "Ultrasonic arrays for non-destructive evaluation: A review," *NDT Int.*, vol. 39, pp. 525–541, Oct. 2006.

[3] C. Li, D. Pain, P. D. Wilcox, and B. W. Drinkwater, "Imaging composite material using ultrasonic arrays," *NDT Int.*, vol. 53, pp. 8–17, Jan. 2013.

[4] S. Deydier, N. Leymarie, P. Calmon, and V. Mengeling, "Modeling of the ultrasonic propagation into carbon-fiber-reinforced epoxy composites, using a ray theory based homogenization method," *Rev. Prog. Quant. Nondestruct. Eval.*, vol. 25, pp. 972–978, 2006.

[5] R. J. Huang, L. W. Schmerr, and A. Sedov, "Modeling the radiation of ultrasonic phased-array transducers with Gaussian beams," *IEEE Trans. Ultrason. Ferroelectr. Freq. Control*, vol. 55, pp. 2692–2702, Dec. 2008.

[6] W. T. Thompson, "Transmission of elastic waves through a stratified solid medium," *J. Appl. Phys.*, vol. 21, no. 2, pp. 89–93, 1950.

[7] N. A. Haskell, "The dispersion of surface waves on multilayered media," *Bull. Seismol. Soc. Am.*, vol. 43, no. 1, pp. 17–34, 1953.

[8] L. Knopoff, "A matrix method for elastic wave problems," *Bull. Seismol. Soc. Am.*, vol. 54, no. 1, pp. 431–438, 1964.

[9] A. H. Nayfeh, "The general problem of elastic wave-propagation in multilayered anisotropic media," *J. Acoust. Soc. Am.*, vol. 89, pp. 1521–1531, Apr. 1991.

[10] A. H. Nayfeh, *Wave Propagation in Layered Anisotropic Media With Applications to Composites*. vol. 1, Amsterdam, The Netherlands: Elsevier Science, 1995.

[11] M. J. S. Lowe, "Matrix techniques for modeling ultrasonic waves in multilayered media," *IEEE Trans. Ultrason. Ferroelectr. Freq. Control*, vol. 42, pp. 525–542, Jul. 1995.

[12] L. Wang and S. I. Rokhlin, "Stable reformulation of transfer matrix method for wave propagation in layered anisotropic media," *Ultrasonics*, vol. 39, no. 6, pp. 413–424, 2001.

[13] S. I. Rokhlin and L. Wang, "Ultrasonic waves in layered anisotropic media: Characterization of multidirectional composites," *Int. J. Solids Struct.*, vol. 39, pp. 4133–4149, Aug. 2002.

[14] S. I. Rokhlin and L. Wang, "Stable recursive algorithm for elastic wave propagation in layered anisotropic media: Stiffness matrix method," *J. Acoust. Soc. Am.*, vol. 112, pp. 822–834, Sep. 2002.

[15] L. Wang and S. I. Rokhlin, "Ultrasonic wave interaction with multidirectional composites: Modeling and experiment," *J. Acoust. Soc. Am.*, vol. 114, pp. 2582–2595, Nov. 2003.

[16] M. J. Mienczakowski, A. K. Holmes, and R. E. Challis, "Modeling of ultrasonic wave propagation in composite airframe components," *Rev. Prog. Quant. Nondestruct. Eval.*, vol. 27, pp. 995–1001, 2008.

[17] T. Pialucha and P. Cawley, "An investigation of the accuracy of oblique-incidence ultrasonic reflection coefficient measurements," *J. Acoust. Soc. Am.*, vol. 96, pp. 1651–1660, Sep. 1994.

[18] B. Hosten and M. Castaings, "Surface impedance matrices to model the propagation in multilayered media," *Ultrasonics*, vol. 41, pp. 501–507, 2003.

[19] J. W. Goodman, *Introduction to Fourier Optics*, 2nd ed., Singapore: McGraw-Hill, 1968.

[20] E. G. Williams, *Fourier Acoustics: Sound Radiation and Nearfield Acoustical Holography*. London, UK: Academic Press, 1999.

[21] A. U. Rehman, C. Potel, and J. F. de Belleval, "Numerical modeling of the effects on reflected acoustic field for the changes in internal layer orientation of a composite," *Ultrasonics*, vol. 36, no. 1–5, pp. 343–348, 1998.

[22] L. W. Schmerr and S. J. Song, *Ultrasonic Nondestructive Evaluation Systems: Models and Measurements*. New York, NY: Springer, 2007.

[23] A. L. Lopez-Sanchez, H. J. Kim, L. W. Schmerr, and A. Sedov, "Measurement models and scattering models for predicting the ultrasonic pulse-echo response from side-drilled holes," *J. Nondestruct. Eval.*, vol. 24, pp. 83–96, Sep. 2005.

[24] A. J. Niklasson and S. K. Datta, "Scattering by an infinite transversely isotropic cylinder in a transversely isotropic medium," *Wave Motion*, vol. 27, pp. 169–185, Feb. 1998.

[25] P. D. Wilcox and A. Velichko, "Efficient frequency-domain finite element modeling of two-dimensional elastodynamic scattering," *J. Acoust. Soc. Am.*, vol. 127, pp. 155–165, Jan. 2010.

[26] A. Velichko and P. D. Wilcox, "A generalized approach for efficient finite element modeling of elastodynamic scattering in two and three dimensions," *J. Acoust. Soc. Am.*, vol. 128, pp. 1004–1014, Sep. 2010.

[27] J. Zhang, B. W. Drinkwater, P. D. Wilcox, and A. J. Hunter, "Defect detection using ultrasonic arrays: The multi-mode total focusing method," *NDT Int.*, vol. 43, pp. 123–133, Mar. 2010.

[28] A. Stovas and B. Arntsen, "Vertical propagation of low-frequency waves in finely layered media," *Geophysics*, vol. 71, pp. T87–T94, May-Jun. 2006.

[29] A. Stovas, M. Landro, and P. Avseth, "AVO attribute inversion for finely layered reservoirs," *Geophysics*, vol. 71, pp. C25–C36, May-Jun. 2006.

[30] G. E. Backus, "Long-wave elastic anisotropy produced by horizontal layering," *J. Geophys. Res.*, vol. 67, no. 11, pp. 4427–4440, 1962.

[31] G. W. Milton, *The Theory of Composites*. New York, NY: Cambridge University Press, 2002.

[32] R. Huang and L. W. Schmerr, "Characterization of the system functions of ultrasonic linear phased array inspection systems," *Ultrasonics*, vol. 49, pp. 219–225, Feb. 2009.

[33] S. I. Rokhlin, W. Huang, and Y. C. Chu, "Ultrasonic scattering and velocity methods for characterization of fiber-matrix interphases," *Ultrasonics*, vol. 33, pp. 351–364, Sep. 1995.

[34] M. Deschamps and C. Bescond, "Numerical-method to recover the elastic-constants from ultrasound group velocities," *Ultrasonics*, vol. 33, pp. 205–211, May 1995.

[35] K. Balasubramaniam and S. C. Whitney, "Ultrasonic through-transmission characterization of thick fibre-reinforced composites," *NDT Int.*, vol. 29, pp. 225–236, Aug. 1996.

[36] B. Hosten, "Stiffness matrix invariants to validate the characterization of composite-materials with ultrasonic methods," *Ultrasonics*, vol. 30, no. 6, pp. 365–371, 1992.

[37] S. I. Rokhlin and W. Wang, "Double through-transmission bulk wave method for ultrasonic phase-velocity measurement and determination of elastic-constants of composite-materials," *J. Acoust. Soc. Am.*, vol. 91, pp. 3303–3312, Jun. 1992.

[38] G. W. Postma, "Wave propagation in a stratified medium," *Geophysics*, vol. 20, no. 4, pp. 780–806, 1955.

[39] R. Huang, L. W. Schmerr, and A. Sedov, "The Kirchhoff and Born approximations for scattering in both isotropic and anisotropic elastic solids," *Rev. Prog. Quant. Nondestruct. Eval.*, vol. 820, pp. 49–56, 2006.

[40] R. J. Huang, L. W. Schmerr, A. Sedov, and T. A. Gray, "Kirchhoff approximation revisited—Some new results for scattering in isotropic and anisotropic elastic solids," *Res. Nondestruct. Eval.*, vol. 17, pp. 137–160, Jul.-Sep. 2006.

[41] M. Castaings, Laboratoire de Mécanique Physique, University of Bordeaux 1, France, private communication. Jul. 2010.

[42] B. Hosten and M. Castaings, "Transfer-matrix of multilayered absorbing and anisotropic media—Measurements and simulations of ultrasonic wave-propagation through composite-materials," *J. Acoust. Soc. Am.*, vol. 94, pp. 1488–1495, Sep. 1993.

[43] B. G. Martin, "Ultrasonic wave propagation in fiber-reinforced solids containing voids," *J. Appl. Phys.*, vol. 48, no. 8, pp. 3368–3373, 1977.

Yousif Humeida received his B.Sc. degree in electrical and electronic engineering from the University of Khartoum, Sudan, in 2007, and an M.Sc. degree in electronic communication and computer engineering from the University of Nottingham, UK, in 2010. From 2007 to 2009, he worked as a Teaching Assistant in Electrical and Electronic Engineering at the University of Khartoum. During this work, he was a Research Associate at the University of Nottingham, pursuing studies toward a Ph.D. degree. He is currently a Research Associate in the Mechanical Engineering Department, University of Bristol. His main interest is the

modeling of ultrasonic signals in solids, especially multilayer anisotropic materials.

Valerie J. Pinfield studied natural sciences (theoretical physics) at the University of Cambridge, UK, and her Ph.D. work was carried out at the University of Leeds Food Science Department on the computational modeling of emulsion instability and ultrasonic propagation in scattering systems. Having worked for a period in research and development in the confectionery industry, she returned to academia to study ultrasonic scattering models and their application in food/pharma systems and advanced materials, first at the University of Leeds and subsequently at the University of Nottingham. Currently, her research interests are in the physical processes involved in acoustic propagation through multiphase systems, and in the modeling of such processes both analytically and numerically. During the work reported here, she was a Senior Research Fellow at the University of Nottingham; she is now a Lecturer in the Chemical Engineering Department at Loughborough University, UK. She is a Chartered Physicist.

Richard E. Challis graduated in electrical engineering from Imperial College, London, in 1967. He returned to Imperial College and received his Ph.D. degree in the applications of engineering to medicine in 1975. He subsequently worked as a clinical engineer at Guy's Hospital, London, and in 1978 was invited to take up a position of professor visitante in the postgraduate engineering division of the Federal University of Rio de Janeiro. In 1980, he returned to the University of London as a lecturer in bioengineering and physiology. Later, he became professor of engineering physics at Keele University and in 1998 moved to the University of Nottingham as head of the School of Electrical and Electronic Engineering. He is a Fellow of the Institution of Engineering and Technology (erstwhile IEE), the Institute of Physics, and the British Institute of Non-Destructive Testing. He was elected a Fellow of the Royal Academy of Engineering in 2004.

Paul D. Wilcox was born in Nottingham, England, in 1971. He received an M.Eng. degree in engineering science from the University of Oxford, Oxford, England, in 1994 and a Ph.D. from Imperial College, London, England, in 1998.

From 1998 to 2002, he was a Research Associate in the Non-Destructive Testing (NDT) research group at Imperial College, where he worked on the development of guided wave array transducers for large area inspection. From 2000 to 2002, he also acted as a Consultant to Guided Ultrasonics Ltd., Nottingham, England, a manufacturer of guided wave test equipment.

Since 2002, Prof. Wilcox has been at the University of Bristol, Bristol, England, where he is a Professor in Dynamics and an EPSRC Advanced Research Fellow. His current research interests include long-range guided wave inspection, structural health monitoring, array transducers, elastodynamic scattering, and signal processing.

Chuan Li received the B.Eng., M.Sc. and Ph.D. degrees in electronic engineering from the University of Warwick, UK, in 2004, 2005, and 2009, respectively. His early research interests included ultrasonic communications using electrostatic transducers and infrared communications. He is now a postdoctorate researcher in the Department of Mechanical Engineering, University of Bristol, UK. His current research is focused on the nondestructive testing of composite material using ultrasonic phased arrays and the development of advanced post-processing imaging algorithms.